Hydrothermal sintering for densification of silica. Evidence for the role of water

Arnaud Ndayishimiye, Alain Largeteau, Stéphane Mornet, Mathieu Duttine, Marie-Anne Dourges, Dominique Denux, Marc Verdier, Mohamed Gouné, Thomas Hérisson de Beauvoir, Catherine Elissalde, et al.

Hydrothermal Sintering for Densification of Silica.

Evidence for the Role of Water

Arnaud Ndayishimiye[1], Alain Largeteau[1], Stéphane Mornet[1], Mathieu Duttine[1], Marie-Anne Dourges[2], Dominique Denux[1], Marc Verdier[3], Mohamed Gouné[1], Thomas Hérisson de Beauvoir[1], Catherine Elissalde[1], Graziella Goglio[1,*]

[1] CNRS, Univ. Bordeaux, ICMCB, UPR 9048, 87 avenue du Dr A. Schweitzer, F-33608 Pessac, France
[2]ISM, UMR CNRS 5255, Univ. Bordeaux, 351 Cours de la Libération, 33405 Talence Cedex, France
[3]Univ. Grenoble Alpes, CNRS, Grenoble INP, SIMAP, F-38000 Grenoble, France

Corresponding author : graziella.goglio@u-bordeaux.fr
Tel : +33 (0)5 40 00 63 34
Fax : + 33 (0)5 40 00 27 61

Abstract

We present hydrothermal sintering as a smart route to densify ceramics at low temperature. Home-made silica nanoparticles naturally hydrated, partially and *quasi*-fully dehydrated were submitted to hydrothermal sintering (190 MPa, 300 °C, 90 min) without additional water. Their morphology and surface chemistry strongly influence their packing and then the mechanical-chemical effects responsible for densification involving dissolution-precipitation mechanisms. The connection between the porosity and the starting compact packing was pointed out. Moreover, the influence of additional chemical effects was highlighted as the polycondensation of protruding silanols favors the formation of interparticle necks *via* the creation of polysiloxane bonds. When external water is added, the filling of the mesopores is nearly fully achieved but large residual macropores initiated in the early stage of sintering are remaining. The compactness of the as-obtained ceramic is 73.6%. We also demonstrate the influence of water on the mechanical and deformation behavior of the samples.

Key words:

hydrothermal sintering, silica, ceramics, low temperature processing densification, mechanical-chemical effects, polycondensation

Introduction

Advanced materials such as new high performance ceramics are our allies for a sustainable future. Their development is strongly dependent on the mastery of efficient sintering processes. Among the different sintering techniques, the most conventional one uses powders as starting materials and densification is performed above 1000 °C to reach at least 95 % of theoretical densities. The reduction of surface free energy, which is the driving force for sintering, might be promoted either by applying pressure[1, 2] or by enhancing diffusional processes in solid[3] or in liquid phase[4] with *ultra*-fast heating routes and/or using nanopowders as starting materials. Consequently many highly performant techniques were developed such as hot pressing, hot isostatic pressing, spark plasma sintering or microwave sintering.[5–12] If it is clearly admitted that pressure is beneficial for densification via particle rearrangement and sliding, plastic deformation and pore shrinkage, the high temperatures usually required in these processes listed above lead to several technological barriers: (i) to ensure the feasibility of their industrial scalability, sintering processes need to be energy-saving and cost effective, (ii) the use of nanopowders as starting materials may yield microstructure with overly coarse grains, which is detrimental to densification, (iii) these high temperatures are not suitable to sinter materials that are metastable or that decompose at low temperature, (iv) co-sintering of multimaterials is hindered by differences in thermal stability, the rate and the onset temperature of shrinkage, and the physical and/or chemical compatibilities between components.

There is then an indisputable interest to develop low temperature ($T < 400$ °C) efficient sintering process to overcome these technological limitations. In this way, processes involving hydrothermal conditions are expected to enhance the reactivity. Recently, interesting results were obtained with Reactive Hydrothermal Liquid-Phase Densification (rHLPD) route to densify barium titanate/titania composites.[13] Based on principles of hydrothermal reaction, infiltration, reactive crystallization, and liquid-phase sintering, rHLPD allowed Riman et al. to obtain a composite with 90% of relative density at 240°C. In June 2016, Clive Randall *et al.* from Penn State University have reported impressive results, reaching 95% of compactness on a large panel of ceramics and composites, with a process named cold sintering process (CSP), inspired from hydrothermal sintering.[4, 14–18] The explored temperature and pressure ranges were 25-300°C and 50-500 MPa, respectively. In 2017, Bouville and Studart for ETH Zurich have claimed the densification of vaterite at room temperature with CSP, hence confirming the high performances offered by this process.[19]

In this context, we have focused on hydrothermal sintering process as a relevant and affordable solution to overcome standard technological limitations. The first experiments were claimed by D.M. Roy *et al.* in the 70's[20, 21] for the preparation of cement pastes that had excellent mechanical properties and almost zero porosity. Then, further studies were made on reactive hydrothermal sintering to produce sintered oxides from metals by hydrothermal oxidation.[22, 23] In the 80's Yamasaki and Yanagisawa improved the hydrothermal hot pressing apparatus and claimed the sintering of silica.[24] This technique was further set up to densify metastable materials (anatase),[25, 26] materials with mild temperature decomposition ($Ca/SrCO_3$,[27, 28] hydroxyapatite[29]), porous ceramics (porous hydroxyapatite,[30] zeolites[31]), nanomaterials without coarsening ($Sn_{1.24}Ti_{1.94}O_{3.66}(OH)_{1.50}F_{1.42}$),[32] amorphous nanomaterials (SiO_2),[33, 34] tailored thermoelectric materials ($Ca_3Co_4O_9$,[35, 36] $Na_xCo_2O_4$[37]) or to bond different materials (hydroxyapatite bonded to titanium,[38] or to magnesium alloy[39]). Hydrothermal sintering is fully inspired from the natural densification *via* geological and biological mineralization processes. Here, a powder with water is externally and mechanically compressed into an autoclave, under hydrothermal conditions (100°C < T < 350°C; 22.5 MPa <P) over short periods of time (from a few minutes to a few hours). The water is expelled during densification and recovered in specific spaces for water retreat. The main driving force of such a process is the stress gradient within particles induced by external uniaxial compression, which allows the activation of the dissolution/precipitation phenomena at the solid/liquid interface.[17] Here, water both acts as a solvent and a mass transport medium, and enhances creep at the solid/solid interface to promote densification. The dissolution occurs in the contact zone between particles while the precipitation operates at the less stressed surface of particles, *i.e.* the surface of pores. The complexity of these mechanical and chemical effects and their coupling have been clearly pointed out.[17] In this way, because the efficiency of densification is driven by the stress gradient in the contact zone between particles, the key role of the particles packing in the initial stage of the sintering is clearly emphasized. Moreover, the surface chemistry of these starting particles is an important lever to tune as the hydrophilicity at the surface will strongly influence the water distribution and the dissolution and precipitation steps. Controlling these features would allow a better understanding and an optimization of the densification.

The main objective of this work is thus to evidence the role of water in the densification mechanisms of silica nanoparticles. Our strategy is to use spherical and monodisperse SiO_2 home-made nanoparticles in order to favor their spontaneous self-organization in the green compact. A partial or *quasi*-full dehydration of these particles will be performed in order to

understand the role of natural hydration, including both physisorbed and chemisorbed water, in the sintering process. A comparison will be made on the mechanisms involved when sintering is performed in presence of additional water. Combining complementary characterizations at different scales, a deep investigation will allow to properly describe the surface chemistry and the microstructure of the nanoparticles and/or of the ceramic at different steps of the process in order to propose sintering mechanisms that take place at the atomic level. The role of mechanical-chemical and chemical effects will be then discussed.

I. Experimental details

Silica nanoparticles:

Synthesis Silica nanoparticles are synthesized following a process described by Hartlen et al.[40] A silica nanoparticle dispersion is prepared in a 1 L vial by adding first 0.535 g of L-arginine (Sigma Aldrich, 99 %) to 407 mL of high purity deionized water (18.2 MΩ.cm produced using Millipore A10 Milli-Q) while thoroughly mixing the solution. Then 26.6 mL of cyclohexane (Sigma Aldrich, 99.5 %) are added to the water-arginine solution and the reaction is heated at 60 °C in a water bath under magnetic stirring at a 150 rpm rate, while keeping the top layer relatively undisturbed. The role of the cyclohexane layer is to control the addition rate of tetraethylorthosilicate (TEOS) into the reaction medium during the nucleation and growth of silica nanoparticles. Once the solution reaches 60 °C, 65.934 mL of TEOS (Sigma Aldrich, 98 %) are added into the vial. A constant stirring and temperature are then maintained for 48 h. The silica nanoparticles are recovered by decantation, vacuum evaporation and dried in an oven at 70 °C for 72 h under air atmosphere. A powder, named SiO_2-NC, is as-obtained.

Nanoparticle partial dehydration : The amount of water in the as-synthesized SiO_2-NC particles is tuned by calcination at different temperatures during 4 h with 10 °C/min heating and cooling rates using a Carbolite CWF 1300 furnace under air atmosphere. Two additional powder batches are consequently obtained: SiO_2-200 and SiO_2-400 corresponding to SiO_2-NC powders that underwent calcination at 200 °C and 400 °C, respectively. The amorphous character of SiO_2-NC, SiO_2-200 and SiO_2-400 is confirmed by X-Ray diffraction.

Hydrothermal Sintering experiments:

(i) Description of the apparatus: The hydrothermal sintering device is a home-made apparatus.[41] In our experiments, 2 g of powdered sample are introduced into a hot pressure chamber and then uniaxially compressed via two push rods equipped with Teflon gaskets to prevent water leakage and to guarantee hydrothermal conditions. The design of the push rods includes a space for collecting water that is expelled by the material during densification (Fig. 1). The uniaxial force is provided using a manually controlled hydraulic pump. The system is heated with a furnace consisting of two resistors in series as a ceramic collar with a 220 V voltage converter used to regulate the temperature. The temperature is measured using a thermocouple placed close to the sample and pressure is read on a manometer.

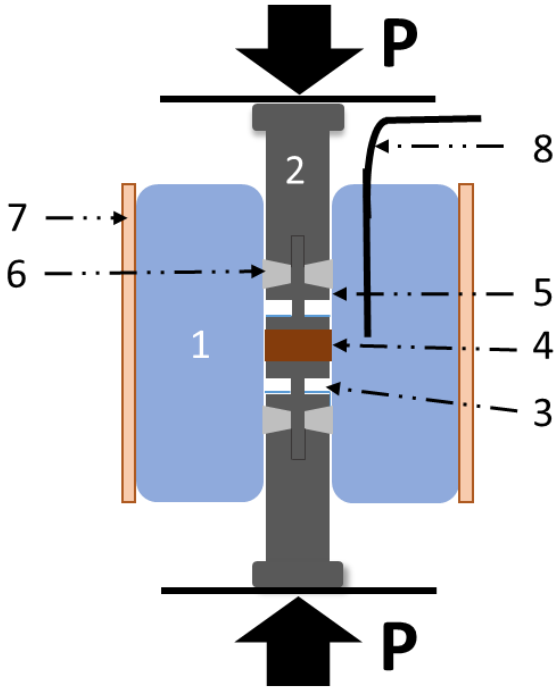

Fig. 1. Schematic representation of hydrothermal hot pressing apparatus. (1) High pressure cylinder, (2) Piston rod, (3) Space for water retreat, (4) Sample, (5) Piston obturator, (6) Teflon gaskets, (7) Ceramic coil, (8) Thermocouple

(ii) Sintering without additional water: starting samples consist in silica nanoparticle powders either naturally hydrated (SiO_2-NC) or partially dehydrated (SiO_2-200 or SiO_2-400).

In a first step, pressure is increased up to 95 MPa in order to favor the rearrangement of the nanoparticle packing in the high pressure chamber and to avoid the vaporization of water during the subsequent heating of the system. Temperature is then increased up to 300°C with a heating rate of 10°C/min. When the maximum temperature is reached, pressure is increased up to 190 MPa. The sample is maintained into the autoclave at 300°C under 190MPa for 90 min. Finally,

pressure is released as the system is naturally cooled down. From SiO_2-NC, SiO_2-200 and SiO_2-400 starting powders, as-obtained sintered pellets are called P-SiO_2-NC, P-SiO_2-200 and P-SiO_2-400, respectively.

(iii) Sintering with additional water: In this case, the sample consists of 2 g of naturally hydrated silica powder (SiO_2-NC) mixed in a mortar with 1.5 mL of additional water (43 wt%). Same sintering procedure as that described in (ii) is followed. One should notice that a small quantity of water is expelled into the space dedicated to water retreat during the precompaction step, the amount of remaining added water within the powder ranging between 35 and 42wt%.

Characterizations of silica nanoparticles and hydrothermally sintered ceramics

Transmission Electron Microscopy (TEM) was performed using a JEOL JEM 1400 to probe the morphology and the size of nanoparticles. Samples are prepared from dried particles mixed with ethanol; a drop of the poorly concentrated suspension is deposited onto copper grids coated with carbon layer (CF300-Cu, EMS Corp.) and let to evaporate at room temperature. Particle sizes and standard deviation are obtained by averaging diameters of about 300 particles measured with Image J software.[42]

High Resolution Scanning Electron Microscopy (HRSEM) was performed on a SEM-JEOL-6700 that operates at an accelerating voltage of 3 kV. SEM images are made on fractures of bulk densified samples. As silica is a non-conducting material, the sputtering of samples with a gold/palladium alloy was required prior to HRSEM observations.

Thermal behavior of the sample is characterized by *ThermoGravimetric Analysis- Mass spectroscopy (TGA-MS*). 25.0 mg of sample are poured in an alumina crucible and measured under air flow with a SETARAM TAG 2400 equipment coupled with a BALZER THERMOSTAR mass spectrometer. The onset temperature of each mass loss is determined at the local maximum of the derivative curve dTG/dt.

Fourier Transformed Infrared Spectroscopy (FTIR) was used to determine the chemical features of both the starting nanoparticles and the sintered materials. It is performed with a single reflection ATR accessory Shimadzu FTIR-8400S. Spectra are obtained from an average of 40 scans in the wavelength range of 500-4000 cm^{-1} in transmittance mode.

The specific surface areas of samples were measured with a Micromeretics ASAP 2010 equipment (Micromeretics Corp., Norcross, USA) after degassing each sample at 150 °C in vacuum for several hours to reach a constant pressure lower than 10µm Hg. *Mercury intrusion porosimetry (MIP)* was used to determine the porosity and pore size distribution of sintered materials. It is performed with a Micromeretics Autopore IV 9500 porosimeter and with following mercury characteristics : contact angle, surface tension and maximum intrusion pressure of 130°, 485 mN/m and 224 MPa, respectively. MIP was also used to determine the bulk density (ρ_b) performing the mercury infiltration at very low pressure (0.0102 MPa). Skeletal density (ρ_s) is measured with an Ultrapycnometer 1000 helium pycnometer (Quantachrome Corp., USA). The relative density (ρ_r) was determined by the ratio ρ_b / ρ_s (%).

Solid-State Nuclear Magnetic Resonance (NMR) measurements were performed with a Bruker Avance III WB 500 MHz spectrometer (11.7 T) equipped with a dual resonance 2.5 mm CPMAS probe. ^{1}H NMR spectra are recorded under magic-angle-spinning (MAS, ω_r=30 kHz) with 2.5 µs ($\pi/2$) pulses and a 5 s recycle delay. ^{1}H to ^{29}Si cross polarization (CP) NMR spectra are recorded under 10 kHz MAS with 3.8 µs pulses, a recycle delay of 4.5 s and contact time ranging from 3 ms up to 20 ms. Chemical shifts (δ) are expressed in parts per million (ppm) with respect to TMS (tetramethylsilane, $\delta(^{1}H)$=0 ppm and $\delta(^{29}Si)$=0 ppm).

The nano-indentation measurements are performed on MTS Nano Indenter XP system. In this study, the methodology used is based on standard Oliver and Pharr analysis[41] using continuous stiffness measurements (CSM) at 45Hz and 2nm oscillation amplitude. The tests are performed at room temperature with a Berkovitch indenter. Tip area calibration and frame stiffness are achieved on fused SiO_2 sample as described by Oliver and Pharr.[43] The samples are carefully polished in both sides in order to limit the effects of surface hardening and to have a flat surface. The hardness is extracted as a mean value between 480 and 500 nm penetration depths, on an average of three to five indents, measured on a surface sample representative of the materials's global microstructure. It is worth noting that the hardness of the sample P-SiO_2-200 could not be measured as it broke into very small and unusable pieces during polishing.

II. From starting silica nanoparticles to hydrothermally sintered samples

II.1. Microstructure and surface chemistry of starting silica nanoparticles

The morphology of the three silica powders was characterized by TEM (Fig.2). Whatever the sample, the nanoparticles are spherical, monodisperse and we do not observe any aggregation phenomena (see Fig. S1, supplementary data) even after thermal treatment at 200 or 400°C. A slight decrease in size of nanoparticles with temperature is observed from 66 nm for SiO_2-NC down to 61 nm in the case of SiO_2-400. This size decrease is consistent with the mesoporous feature of the silica nanoparticles. Indeed, R.T. Baker and J.B. Lowe claimed that this contraction of particles originates from a continuous polycondensation of silanols groups induced by calcination, followed by a collapse of mesopores.[44, 45] This polycondensation which induces the disappearance of the *intra* particle porosity is all the more efficient since the calcination temperature is high, inducing in the case of SiO_2-400, an increase of the specific surface area up to 60±1 $m^2.g^{-1}$ (Table I) compared to that of SiO_2-NC (41±1 $m^2.g^{-1}$).

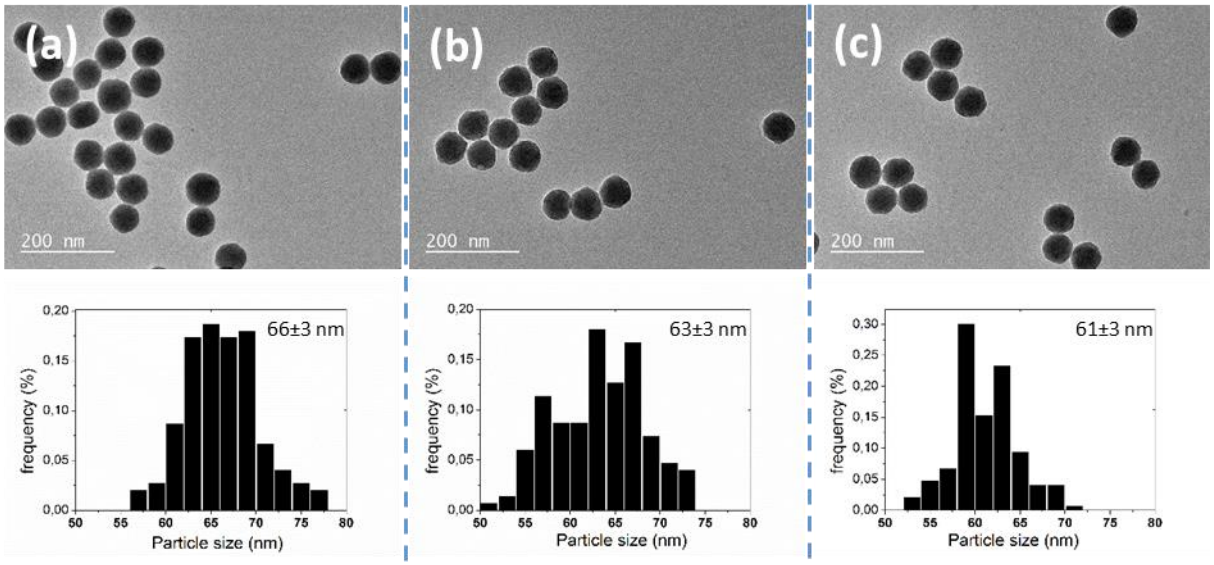

Fig. 2. TEM images of silica nanoparticles and associated statistics on the particle size on a) SiO_2-NC, b) SiO_2-200 and c) SiO_2-400

Considering the surface chemistry of the nanoparticles as a key feature regarding the hydrothermal sintering process, in-depth analysis was performed combining FTIR and NMR spectroscopies with thermal analysis.

The chemical nature of three powdered samples was unambiguously determined as silica by infrared spectroscopy analysis (Fig. 3). The bands at 580, 803 and 1053-1190 cm^{-1} are assigned to Si-O-Si bending, symmetric stretching and asymmetric stretching, respectively.[46–52] Moreover, Si-OH asymmetric stretching band manifests itself by the presence of a shoulder at

978 cm^{-1} hence confirming, as expected, the presence of silanol group. Its intensity slightly decreases with increasing calcination temperature due to the partial thermally induced dehydroxylation. As described by Zhuravlev model,[53] these silanols may be either internal groups inside the silica matrix or groups localized at the particle and *intra* particle mesopore surfaces. In this case, silanols may be isolated, vicinal or geminal. One should also notice, on the SiO_2-NC spectrum, bands at 1650 and 3400-3700 cm^{-1} that are attributed to the H_2O-bending and to stretching vibrations of hydroxyl groups, respectively. These bands have a very low intensity that decreases after the calcination of silica, as expected when dehydration occurs.

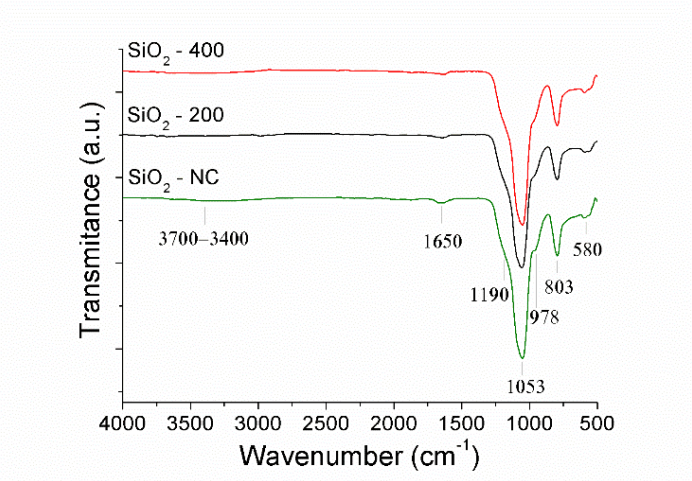

Fig. 3. Infrared spectra of the three starting silica nanoparticle samples

Because the hydroxylation of silica nanoparticles was pointed out by infrared spectrometry, TGA-MS was used to provide a quantitative analysis for the three samples and to evidence any other mass departure (Figure 4, Table I). Three main mass losses are observed with starting temperature around 25 °C, 150 °C and 400 °C. Mass spectrometry analysis reveals since 400 °C the departure of important fractions of CO_2 and NO_x while the water loss observed above this temperature is negligible as frequently observed in the literature.[53, 54] This organic mass departure originates from the final decomposition of L-arginine molecules still present in the powders after the synthesis. This L-arginine decomposition seems to start at 225 °C as small fractions of CO_2 and NO_x are detected but this mass loss remains negligible compared to water departure. As a consequence two main water losses may be roughly estimated while neglecting organic departure below 400 °C. The first event occurring from 25 °C to 150 °C corresponds to the desorption of physically adsorbed water. This departure is observed in the three samples but the water loss is all the more lower when the calcination temperature of the SiO_2-NC powder is higher (2.6, 2.0 and 1.0 wt % for SiO_2-NC, SiO_2-200 and SiO_2-400, respectively). Such

physisorbed water, inherent to the mesoporous nature of silica (see Fig. S2, supplementary data), is not only present at the particle surface[55, 56] but is also trapped into the mesopores.[56–58] From 150 °C, SiO_2-NC and SiO_2-200 undergo a mass loss that is correlated to chemisorbed water release (2.4 and 1.4 wt%, respectively), while this event becomes negligible in the case of SiO_2-400 (0.1%). It was shown that there is a small decrease in silanol group density per surface unit after calcination around 200 °C due to their polycondensation that goes along with the release of chemisorbed water.[53, 54, 59–61] In the temperature range 150-400 °C, at first, both the concentrations of internal and vicinal silanols are expected to predominantly decrease.[54] It is interesting to notice that the higher the chemisorbed water amount is, the higher the physisorbed water quantity is because silanol groups act as adsorption sites for ambient water.[54] For SiO_2-400, the polycondensation of silanol groups proceeds, justifying why there is almost no chemisorbed water left in particles. However, some residual silanol groups remain present up to the calcination temperature at 400 °C as evidenced by IR spectroscopy (Fig. 3).[54, 61]

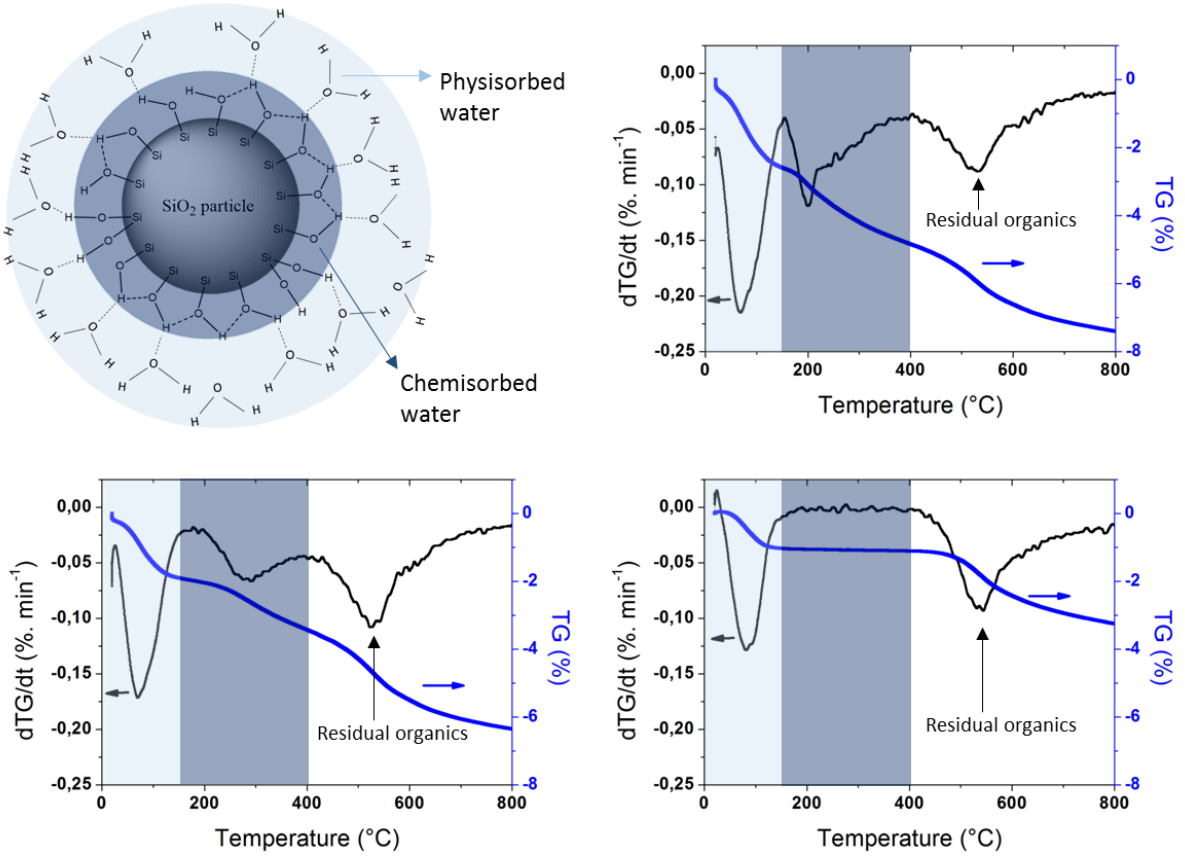

Fig. 4. (a) Schematic representation of a silica nanoparticle. The nanoparticle is mesoporous silica (see Fig. S2, supplementary data). Si-OH groups both internal and localized at the

surfaces of the particle and of the pores. Weight losses and derivative curve with respect to time of powder (b) SiO_2-NC, (c) SiO_2-200, (d) SiO_2-400

The ^{1}H MAS NMR spectra of SiO_2-NC (Fig. 5) exhibit several overlapping signals with isotropic chemical shifts (δ_{iso}) ranging from 1 to 8 ppm depending on the strength of involved hydrogen bonds.[62–64] The narrow and intense signal observed at 1.2 ppm is due to mobile molecular water probably trapped into mesopores whereas the resonance line at about 4 ppm may corresponds to physisorbed water molecules. Weakly bonded hydroxyl groups are responsible for the signal observed at about 5 ppm whereas the broader and more shifted NMR signals (δ_{iso} > 6 ppm) are attributed to internal hydroxyl groups associated with non-bridging oxygen atoms (Si-OH). Silanol groups are located either at the surface (of the particle or of the mesopores) or inside the silica network. In the first case, they act as preferential sites for water physisorption or interact all together with hydrogen bonding which leads to weakly bonded hydroxyl groups. In this way, considering the linear (and empirical) correlation that was evidenced between the ^{1}H chemical shift (δ_{iso}) and the O-H···O distance,[62] fairly weak hydrogen bonds with d(O-H···O) ranging from 2.80 to 2.95 Å are evidenced in all the analyzed silica nanoparticles. The thermal treatments at 200°C and 400°C clearly affect the central part of ^{1}H NMR spectra (3 – 6 ppm), which may be related to the polycondensation of silanol groups and the decrease of chemisorbed water within the silica particles, ensuring consistency with previous observations.

The (^{1}H)^{29}Si CP-MAS NMR experiments allow to transfer the magnetization from the abundant and sensitive ^{1}H spins to the diluted and poorly sensitive ^{29}Si spins during the so-called contact time (typically a few milliseconds), which is a key parameter to improve the ^{29}Si detection.[65-67] Longer contact times are usually required for significantly enhancing the NMR signal of Si nuclei that are the farthest from protons. The (^{1}H)^{29}Si CP-MAS NMR spectra of the SiO_2-NC, SiO_2-200 and SiO_2-400 nanoparticle samples (Fig. 5) show three resonance lines (with Gaussian shape) at about -90, -100 and -110 ppm, which are assigned to distinct Si local environments $Q^{(n)}$ with n=2, 3 and 4 bridging oxygen atoms, respectively.[64, 66, 67] As expected, the CP-MAS signals of Si with hydroxyl groups in its vicinity ($Q^{(2)}$ and $Q^{(3)}$ environments) are enhanced with shorter contact time (3.5 ms) than the $Q^{(4)}$ signal (> 10 ms). This effect is especially evidenced for the heat-treated samples. Indeed, for the SiO_2-200 and SiO_2-400 silica particles, the optimal enhancement of the ^{29}Si NMR signal associated with the $Q^{(4)}$ environment (*ie*. without hydroxyl groups) requires longer contact times (> 15 ms), indicating that the

protons are less numerous and farther from the Si atoms (probably located at the surface or close to the surface of the particles) than for SiO_2-NC. This corroborates the decreasing amount of chemisorbed water molecules and the concomitant polycondensation of silanol groups.

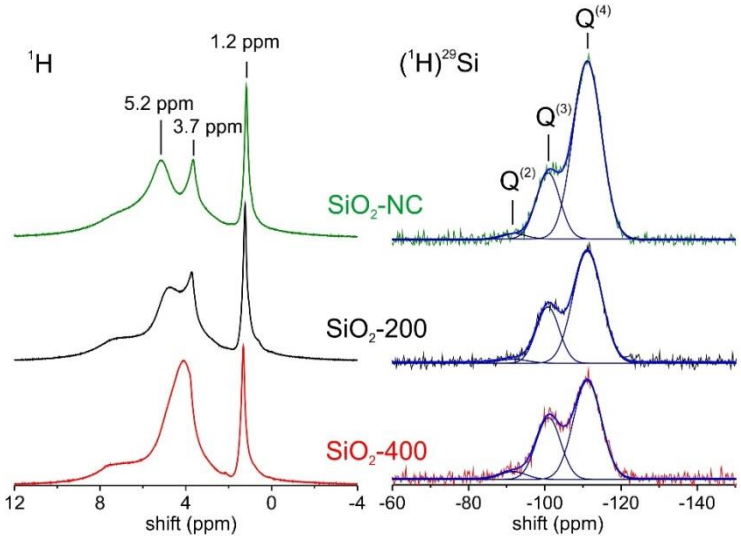

Fig. 5. ^{1}H MAS and (^{1}H)^{29}Si CP-MAS NMR spectra of silica nanoparticles

We have then evidenced the nice sphericity and monodispersity of the silica nanopowders. As expected, the thermal treatment favors the dehydration of the material, either partial of *quasi*-full, depending on the experimental conditions. The departure of physisorbed water is followed by chemical water release induced by the polycondensation of native silanols. The hydrophilicity and reactivity of the starting nanoparticles were then consequently tuned by this thermal treatment.

Table I. Summary of different characteristics of starting powders and hydrothermally sintered samples

	SiO_2-NC		**SiO_2-200**		**SiO_2-400**		**SiO_2-AW**	
	Powder	*sintered*	*Powder*	*sintered*	*Powder*	*sintered*	*Powder*	*sintered*
Bulk density ($g.cm^{-3}$)		1.45		1.44		1.37		1.60
Relative density (%)	-	67.1	-	66.8	-	63.3	-	73.6
Specific surface area ($m^2.g^{-1}$)	41(1)	14(1)	41(1)	36(1)	60(1)	54(1)	-	2.0(5)
wt % $H_2O_{phys.}$	2.6	1	2.0	0.4	1.0	0.6	2.6*	0.2
wt % $H_2O_{chem.}$	2.4	1.2	1.4	0.2	0.1	0.04	2.4*	2.3

wt % H_2O_{total}	5.0	2.2	3.4	0.6	1.1	0.6	5.0*	2.5
vol % mesopores (2-50nm)	-	55	-	88	-	81	-	1
vol % macropores (>50nm)	-	45	-	12	-	19	-	99

** Characteristics of the starting powder before the addition of water (35-42 wt % added)*

II.2. Influence of physisorbed, chemisorbed and additional water on hydrothermal sintering of silica nanoparticles

SiO_2-NC, SiO_2-200 and SiO_2-400 powdered samples were submitted to hydrothermal sintering experiment without any water addition (190 MPa, 300 °C for 90 min), which led to three samples (P-SiO_2-NC, P-SiO_2-200 and P-SiO_2-400, respectively). The same sintering schedule was applied to SiO_2-NC in presence of additional water, sample noted P-SiO_2-AW was as-obtained. The four densified samples remain fully amorphous (as confirmed by X-Ray diffraction) and have the same skeletal density (ρ_s) of 2.17±0.01 g.cm^{-3}, which is consistent with values observed in literature for silica.[68, 69] However the relative densities ρ_r, defined as the ratio ρ_b /ρ_s between the bulk density ρ_b and the skeletal density, are strongly dependent on the starting powder and water addition (73.6 %, 67.1 %, 66.8 % and 63.3 % for P-SiO_2-AW, P-SiO_2-NC, P-SiO_2-200 P-SiO_2-400, respectively, see Table I and Fig. 6). ρ_r increases (*i.e.* the total porosity decreases) while the specific surface area significantly decreases (from 54 m^2.g^{-1} for P-SiO_2-400 down to 14 m^2.g^{-1} for P-SiO_2-NC) with the increasing amount of water in the starting powder. Moreover, the addition of water in the system leads to a significant improvement of the densification as shown by the highest relative density and lowest specific surface area obtained (73.6 % and 2.0 m^2.g^{-1}, respectively, for P-SiO_2-AW). To our knowledge,

this compactness is the highest reported on silica in literature, the best densification (72.7 % of relative density) being previously observed by Yanagisawa *et al.* on submicronic silica after hydrothermal hot pressing at 250°C, 220 MPa during 20 minutes.[34] In our experimental conditions, the higher the water amount is, the more efficient the hydrothermal sintering is. Moreover, whatever the sample and without additional water, the quantity of both physisorbed and chemisorbed water in sintered materials significantly decreases (Table I) while, when water is added, chemisorbed water amount remains unchanged after hydrothermal sintering (physisorbed water quantity becomes negligible). These observations are consistent with the presence of water collected in the space dedicated to water retreat after sintering, additional, physisorbed and chemisorbed water being expelled from the sample during hydrothermal densification.

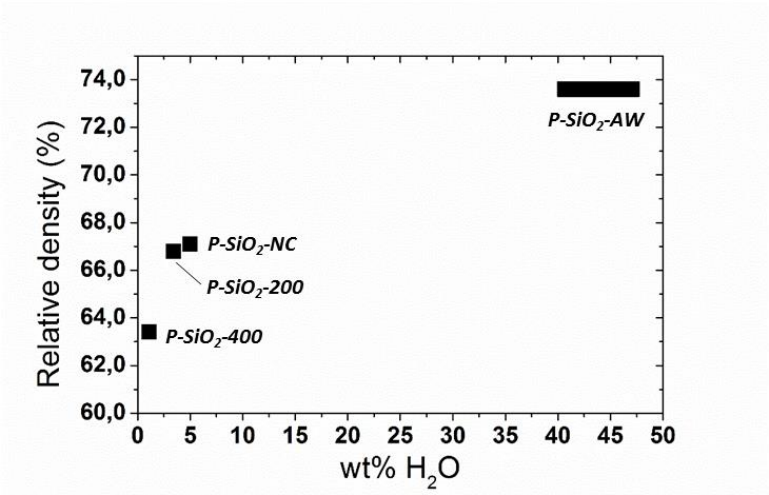

Fig. 6. Relative densities of hydrothermally sintered samples versus the amount of water, taking into account natural hydration and additional water.

In order to evidence and to understand the as-induced modifications of microstructure during sintering, the four sintered samples were characterized by HRSEM (Fig.7).

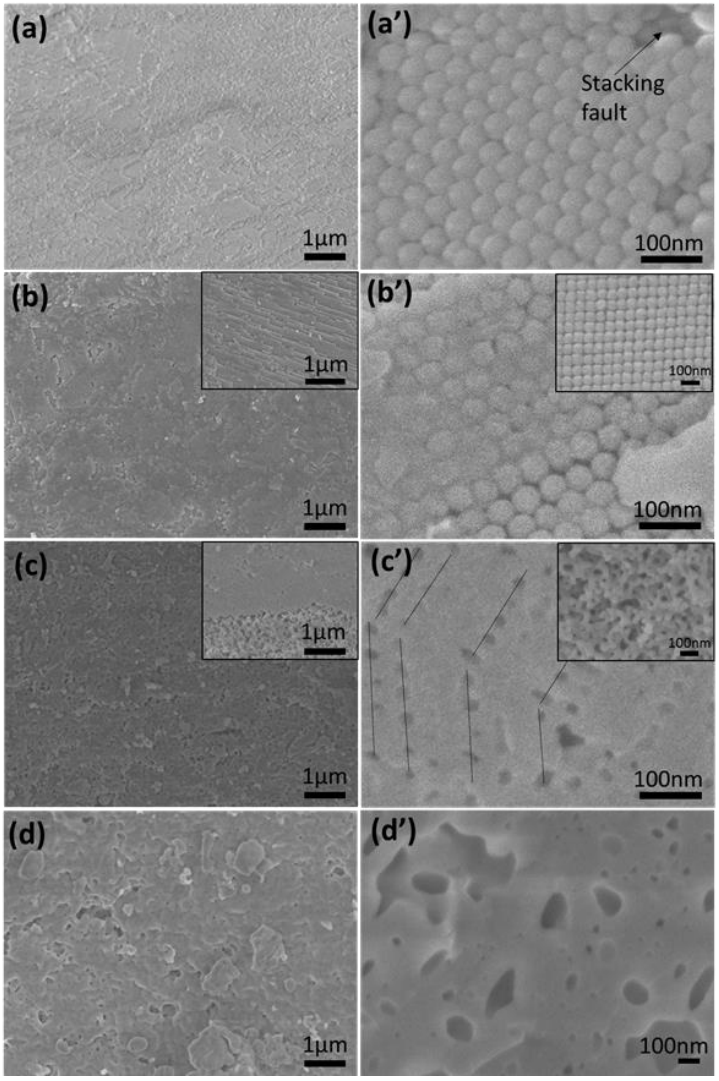

Fig. 7. HRSEM images of (a-a') P-SiO_2-400, (b-b') P-SiO_2-200, (c-c') P-SiO_2-NC and (d-d') P-SiO_2-AW. For images b' and c', minority microstructures are shown in insert. In figure c', the full lines are just a guide-to-the-eye to emphasize the pore organization.

The microstructure significantly evolves with the hydration rate in the starting powders. The P-SiO_2-400 sample exhibits a homogeneous microstructure (Fig. 7a-a') exhibiting an impressive close packing array of silica nanoparticles. Such an organization was previously observed by Yanagiwasa *et al.* in the case of hydrothermal hot pressing of submicronic silica nanoparticles.[34] Some stacking faults are observed as blocks of several neighboring particles are missing. However, at this stage, one could not exclude the possibility of particle removal during the sample preparation for HRSEM (fracture). In this sample, no densification effect is evidenced, *i.e.* the absence of *inter* particle neck growth is in full agreement with the poor evolution of specific surface area evaluated after sintering. In the case of P-SiO_2-200 sample (Fig. 7b-b'),

putting aside the minority cubic stacking of particles, a remarkable nanoparticle close packing is also evidenced, with a layer-by-layer organization observed at the micrometric scale. Similarly to the sample P-SiO_2-400, there is no significant neck formation, stemming from a non-densifying mechanism (see insert of Fig. 7b'). Such well-organized array is surprisingly partially embedded into an amorphous silicic phase, favoring the cohesion of the assembly and inducing a slight decrease of the specific surface area. This glassy phase is not homogeneously distributed within the sample. One can assume that the water amount in the starting sample is sufficient to initiate some dissolution but too low to promote isostatic conditions, hence leading to a non-homogeneous stress gradient at the contact zones. As a result, dissolution can be expected in some preferential directions and/or areas leading to inhomogeneous precipitation. Moreover, this glassy phase is not observed in the cubic stacking zones, which indicates a higher reactivity in mostly strained close packed zones.

In the case of P-SiO_2-NC (Fig. 7c-c'), a multimodal pore size distribution is clearly observed. Highly dense microstructure with residual mesopores is mainly observed all over the sample. However, differential densification is observed, inducing locally a vermicular-type microstructure associated with the presence of macropores (insert of Fig. 7c'). This specific microstructure could be ascribed to several features arising from the initial particle packing : (i) the presence of local initial packing faults that induces reminiscent macropores after sintering [3, 70, 71], (ii) the existence of gradients in the distribution of the radial and axial stress during the powder compression[72, 73], (iii) a heterogeneous water distribution into the sample. However, the nice organization of mesopores observed on Figure 7c' makes reasonable to assume a close packed array of nanoparticles over a large part of the material prior to sintering. In fact, these mesopores should be reminiscent from the *inter* particle interstices in this starting organized assembly. Hence hydrothermal sintering was highly promoted as contacts between particles were enhanced. The basic physical-chemical mechanism of hydrothermal sintering involves dissolution-precipitation process, referred to pressure solution creep in geology, which relies on the transport of matter from the point of contact where the neighboring particles touch to the surrounding liquid phase and eventually to nearby non-contacting surfaces.[74–78] This expected dissolution/precipitation reaction is: $SiO_2 + 2\ H_2O \Leftrightarrow H_4SiO_4$.[79] This transport pathway locally decreases the distance between the centres of the particles, enabling global shrinkage and further densification. The motion of species during pressure solution creep is driven by the high-stress concentration at the contact point (grain boundary) when the compact is subjected to an externally applied mechanical load. In response to such a stress concentration, species at the contact point dissolve from the solid particle into the interfacial solid film and eventually

diffuse along the grain boundary before reaching the continuous liquid phase and precipitating on a lower-stressed particle surface, *i.e.* at the surface of particles into the pores. However, in addition to these mechanical-chemical induced dissolution-precipitation phenomena, one should take into account that, at the atomic level, it has been shown that the adhesion between silica surfaces is clearly enhanced in the presence of a thin layer of water.[80–82] In fact, in contact with this water film, silica surfaces undergo slow structural and chemical changes due to protruding silanol and silicic acid groups that grows on the surface. These groups at the surface of neighboring particles favor the neck formation by reacting chemically to form covalent bridging Si-O-Si bonds.[80] The assumption of siloxane bond formation becomes strongly relevant when considering the decrease of the silanol band concomitant with the appearance of the siloxane band at 670 cm^{-1} observed on the infrared spectrum of the sintered sample P-SiO_2-NC (Fig. 8). On the basis of such observations a mechanistic scenario can be proposed where the pressure solution creep in hydrothermal conditions favors the pore filling by precipitation of silica while the dehydration reaction between silanol groups to form siloxane bridges may favor the formation of necks between particles. The complementarity and synergy of these two phenomena hence promote densification.

Fig. 8. Infrared spectra of SiO_2-NC and P-SiO_2-NC illustrating the evolution of the sample

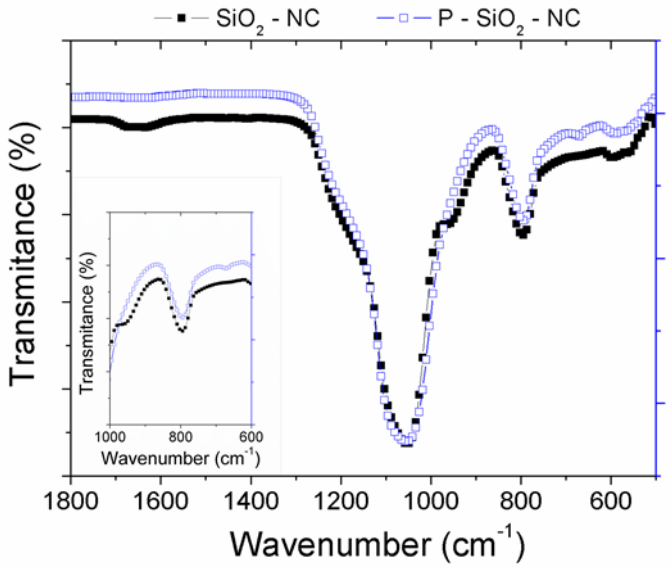

during sintering. The insert focuses on the disappearance of the silanol band at 953 cm^{-1} and the native Si-O-Si siloxane band at 670 cm^{-1} in the sintered sample.

At this stage, the comparative study of the hydrothermal sintering of the three silica powders without additional water has pointed out the nice close packing of the nanoparticles before

sintering. This particle organization is a prerequisite to (i) promote the densifying mechanisms by favoring both the neck formation (siloxane bridges between neighboring particles) and the filling of mesopores (dissolution-precipitation phenomenon induced by *intra* grain stress gradient) and (ii) avoid, into the green material, the presence of macropores that cannot be removed during sintering. Obviously, a minimum amount of initial water is mandatory to initiate the mechanical and chemical effects contributing to densification.

It is therefore consistent to focus on the role of additional water. When water is added, a significant increase in densification and a drastic change in microstructure are observed after hydrothermal sintering (Fig. 7d-d'). Here, in the matrix, no mesopore can be evidenced while a large number macropores of several hundreds of nm in size are observed. The large macropores strongly affect the mechanical properties of P-SiO_2-AW making the sample highly breakable. As a consequence, some fragments, probably removed during the fracture, are observed at the surface of the sample. The absence of reminiscence of both the initial morphology and organization of the nanoparticles attests to an effective densification of the powder. In this specific case, during the compaction step, the addition of water strongly disturbs the natural self-organization of the nanoparticles and the observed removal of the excess of water generates some local turbulences that induce major stacking faults. As ever discussed, once these faults are present in the initial stage of compaction, the reminiscence of macropores within the final sintered sample is unavoidable. Moreover, one could not exclude the possibility of water excess trapping into large pores, due to insufficient water release kinetics with respect to enhanced dissolution/precipitation phenomena. Here, the necessity to optimize the process focusing on both the green density and the initial amount of water appears mandatory to improve the densification. It is worth noting that the very low residual amount of physisorbed water (Table I) is consistent with the decrease of silanol groups by formation of siloxane bridges between neighboring particles, enhancing the formation of necks required for densification.

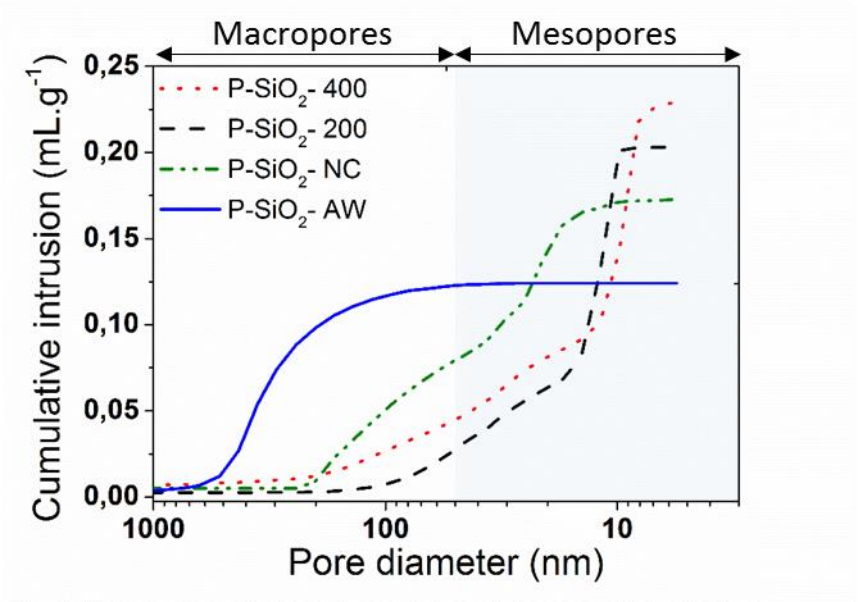

Fig. 9. Cumulative pore intrusion evolution of sintered samples

These microstructural investigation was completed and correlated to the characterization of porosity by mercury porosimetry intrusion (Fig. 9). As expected, the porosity of the four sintered samples is mainly characterized by a distribution of macropores (>50 nm) and/or mesopores (2 nm < pore size < 50 nm)[83], which relative ratio is strongly dependent on the nature of starting powder or on the water addition. First of all, it is clear that the overall porosity is decreasing when the initial water amount (either natural or added) increases. For the less hydrated samples, mesopores are significantly predominant (81 % and 88 % in case of P-SiO_2-400 and P-SiO_2-200, respectively) in comparison to macropores. The majority presence of mesopores is clearly consistent with the interstitial areas in a close-packed assembly of particles. Moreover, macropores whose sizes do not exceed 200 nm could be reasonably assigned to the stacking faults with 1 to 3 neighbor particles missing in the close packing as expected from microstructure observed for example on Figure 7a'. For P-SiO_2-NC, where the starting hydration rate was intermediate, the porosity consists of 45 vol % of macropores and 55 vol % of mesopores (Fig. 9, Table I). On the one hand, the important decrease of mesopore amount originates from the filling of these interstices due to dissolution-precipitation phenomena, while, on the other hand, vermicular-type microstructure is predominantly at the origin of the macropore formation. When water is added, porosity is mostly ascribed to macroporosity (99 % of macropores for P-SiO_2-AW). Hydrothermal sintering has impressively allowed the filling of almost all the initial mesopores while disorganized stacking of primary

particles and probable water trapping leads to macropores. In case of P-SiO_2-AW, the macropores are consequently larger with sizes reaching several hundred of nm. This confirms that water excess release during compression strongly induced a local disorder of the particles in the green material.

The chemical features of sintered samples were investigated by NMR experiments performed on the P-SiO_2-NC and P-SiO_2-AW samples (Fig. 10). ^{1}H MAS NMR spectra clearly shows a decrease of the NMR lines associated with mobile and physisorbed molecular water (at 1.2 ppm and about 4 ppm, respectively) as well as the quasi-disappearance of the internal hydroxyl groups signal (δ_{iso} > 6 ppm). Moreover, the NMR spectrum of the P-SiO_2-AW sample exhibits an intense and narrow line at 4.7 ppm, which is attributed to free water molecules (probably trapped into the large macropores as previously considered).

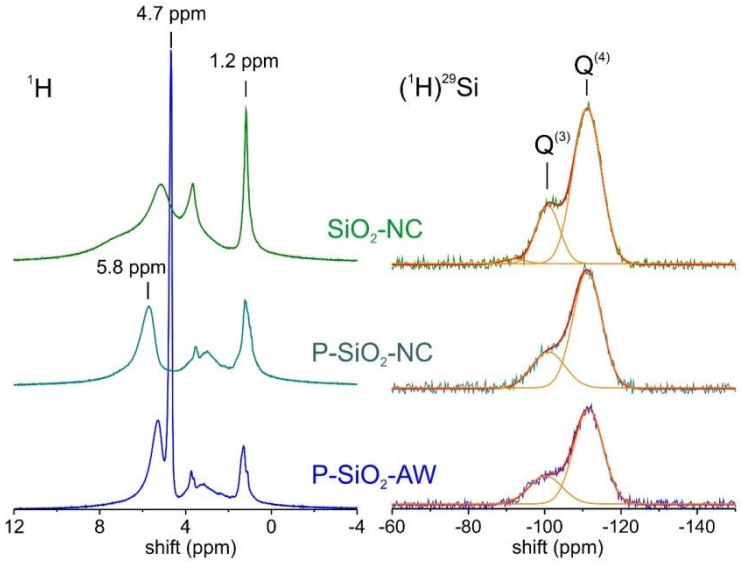

Fig. 10 ^{1}H MAS and (^{1}H)^{29}Si CP-MAS NMR spectra of the raw silica particles (SiO_2-NC) and P-SiO_2-NC and P-SiO_2-AW sintered samples

The (^{1}H)^{29}Si CP-MAS NMR spectra of the sintered samples still exhibit the resonance lines at about -100 and -110 ppm, which are assigned to Q$^{(3)}$ and Q$^{(4)}$ Si local environment, respectively. However, a global decrease of the spectrum intensity is observed and the optimal enhancement of the ^{29}Si NMR signal is achieved with shorter contact times for the sintered samples (10 ms) than for the SiO_2-NC particles (20 ms). Thus, the protons, which can transfer their magnetization to Si nuclei, are probably less numerous but relatively close to the Si atoms. This

may be related to the decreasing amount of silanol groups and physisorbed water after sintering while the content of chemisorbed water molecules remains significant (P-SiO_2- NC) or unchanged (P-SiO_2-AW). The decreasing amount of silanol groups is, at first, related to the disappearance of internal silanols as proposed by Zhuravlev model.[53] Moreover, when no external water is added, physisorbed water acts as a solvent for dissolution-precipitation mechanism and is removed from the sample when densification occurs. The sintering neck creation is related to the formation of siloxane bridges *via* a dehydration reaction, *i.e.* to chemisorbed water departure by condensation of surface silanols. In this case, both physisorbed and chemisorbed water amounts decrease. However, in the vermicular microstructure, one should expect a residual surface hydroxylation. When external water is added, because mesopores have disappeared, one should admit a highly reactive dissolution-precipitation phenomenon, hence expelling physisorbed and most of additional water from the system. By the way, it is interesting to notice that the final amount of water in P-SiO_2-AW remains quite low in comparison to the total amount of water before sintering. Internal silanols disappear according to condensation phenomena, favored by temperature-pressure application. For the same reason, siloxane bridges are formed between particles and at the surface of the macropores. However, because water is trapped into the very large macropores, it induces a surface modification. In this case, a rehydroxylation arises from the dissociative adsorption of water with a splitting of weakened strained surface siloxane bridges, leading to a significant chemisorbed water amount after sintering. One should consider that the more water is added, the more the surface of the particles can be disturbed and modified.

Hence, NMR characterization corroborates previous conclusions, *i.e.* the participation of physisorbed water to dissolution-precipitation hydrothermal sintering mechanism and the decrease of silanol groups by formation of Si-O-Si siloxane bridges, responsible for the formation of sintering necks between particles.

Finally, a correlation between the microstructure of the samples and the mechanical properties is proposed. The hardness curves, measured by nanoindentation on sintered pellets, exhibit two different parts: the surface contribution on the first 50 nm and the volume contribution in the bulk.[84–86] In most cases, the value of surface hardness is indicative of the contact between the indenter tip and the disturbed surface of the sample, resulting from contamination and roughness following polishing. As the displacement into surface increases, the value converges to bulk hardness. The densified pellet P-SiO_2-NC and the compacted pellet P-SiO_2-400 exhibit the same curve shapes, with comparable surface contributions and a nearly constant bulk

contribution. This suggests that both samples have a roughly homogenous microstructure into the measured depth. However, a slight decrease of bulk contribution in P-SiO_2-NC is observed from 500nm to 2000nm. The reason for this is clear and can be mainly attributed to the extrapolated calibration. As expected, P-SiO_2-NC exhibits a higher hardness (2.7±0.5 GPa) than P-SiO_2-400 (1.6±0.3 GPa), which is consistent with the cohesive sintering effects that occurred in P-SiO_2-NC.

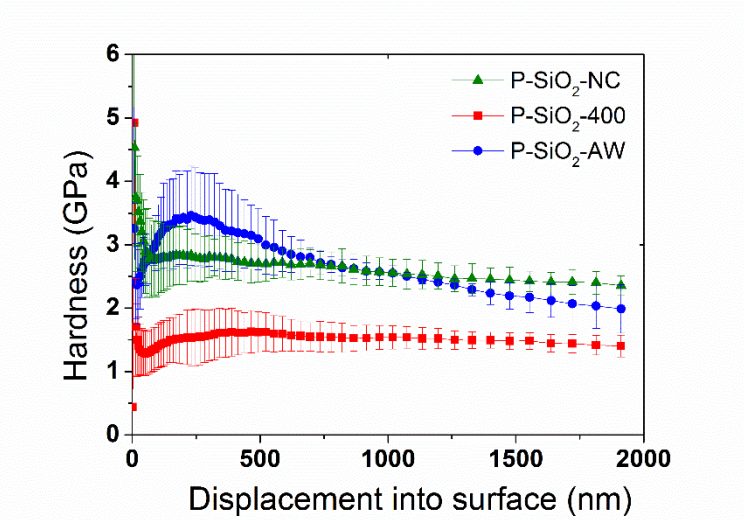

Fig. *11. Hardness versus displacement of sintered pellets obtained by nanoindentation*

It is also interesting to note that P-SiO_2-AW has a different hardness behavior than others samples (Figure 11). Indeed, it has a smaller surface contribution as it cannot adsorb water molecules from ambient air and, as a result, its hardness curve exhibits a different evolution. After an initial increase, a decrease in hardness is observed which is followed by a plateau. This type of evolution has already been observed in reference by Jauffrès *et al.*.[87] It characterizes a rigid-plastic behaviour and would be a consequence of an irreversible deformation by brittle collapse of macropores. Indeed, after an initial elastic-plastic behaviour leading to hardness close to 3.5GPa, the brittle pores collapse under the indenter and the hardness decreases. This phenomenon is however not observed for P-SiO_2-NC while it consists of ~45 vol % of macropores and ~55 vol % of mesopores. This suggests that both size and the relative proportion of pores of different natures may play a key role in mechanical response. The mean value of hardness on the silica matrix of P-SiO_2-AW is 3.1±0.5 GPa, which is a higher than those of the other samples due to more advanced stage of densification. However, in all cases,

the hardness measured is lower than those measured on dense silica glasses obtained by quenching of melt silica.[88, 89] The presence of pores in samples unambiguously explains such a difference. It is thus clearly evidenced that the addition of some water has an indirect influence of both mechanical and deformation behavior.

III. Discussion

Hydrothermal sintering is based upon dissolution reaction, in presence of a solvent, at the highly-stressed contact zones between particles followed by a precipitation on non-contacting lower-stressed surfaces (Fig. 12). This mechanical-chemical induced densification is more efficient when the particles are initially close packed (leading to mesopores in the green material), in order to generate high stress gradients. As a consequence, any stacking faults in the green materials will generate residual macropores in the sintered material. In the case of silica, nanoparticles naturally self-organize during the compaction step however, if water is added in the system, as-induced local turbulences strongly disturb this arrangement and macroporosities are inevitably formed in the ceramic. The amount of water is obviously a crucial parameter in this process. In this way, silica is an interesting material as its native hydroxylation induces an inherent reactivity that it particularly suitable for hydrothermal sintering. The particles raw from synthesis are naturally hydrophilic due to their surface hydroxylation. The physisorbed water acts as the solvent and promotes dissolution-precipitation. However, the presence of residual mesopores after sintering reveals that the process was uncomplete due to an insufficient physisorbed water amount. If physisorbed water is removed from the sample before the sintering experiment, no significant effect is then observed, as expected. On contrary, if additional water is added before sintering, all the mesopores disappear evidencing an efficient densification effect brought to completion in initially close packed areas.

In the case of silica and in addition to these mechanical-chemical effects, one should consider chemical mechanisms enhanced under temperature and/or pressure (Fig. 12). The silanols both internal and at the surface of the particles and of the pores polycondensate hence leading to chemisorbed water departure and to the formation of siloxane bridges in particular between touching particles. This Si-O-Si inter particle bonds promote the sintering neck formation, hence favoring the densification of the material. In presence of a water excess that may be trapped into the macropores, the hydrophobic siloxane surface turns to hydrophilic due to a

rehydration of the surface. A summary of the complementarity and synergy of the mechanical-chemical and chemical effects is schematically depicted in Fig. 12.

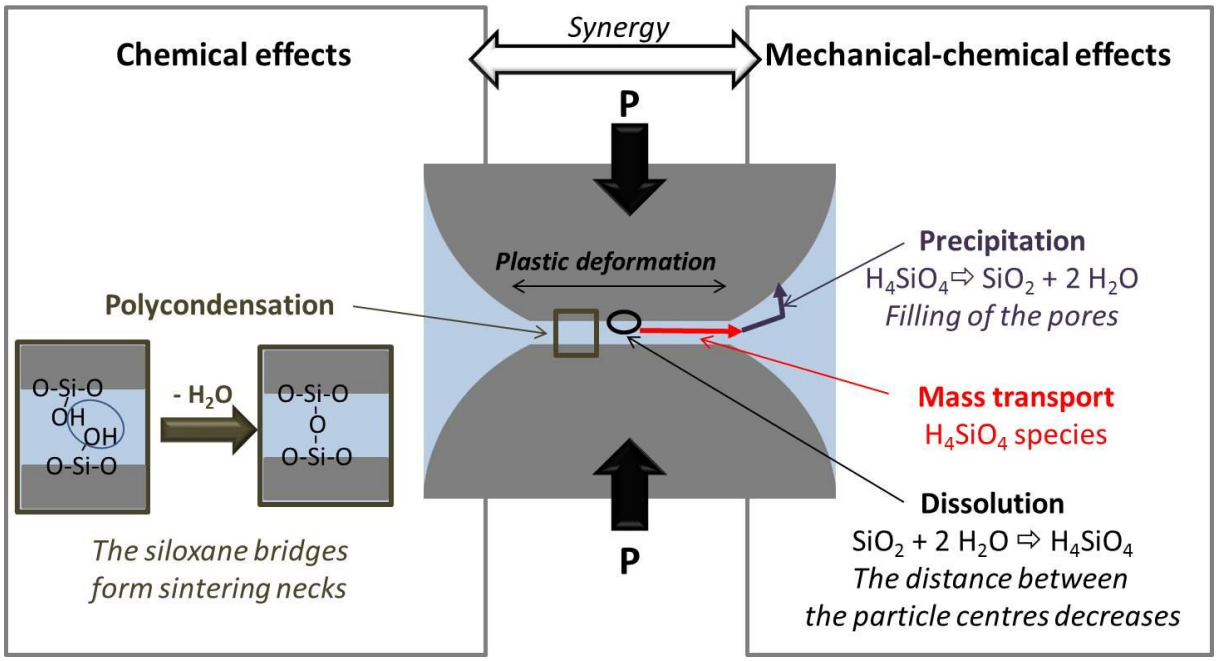

Fig. 12. Influence of mechanical-chemical and chemical effects in hydrothermal sintering process

IV. Conclusion

These results clearly emphasize the potential of hydrothermal sintering, where mechanical-chemical effects can be synergistically assisted by chemical ones. Adding water favors the dissolution-precipitation mechanisms, that become highly efficient as proved by the disappearance of all the mesopores originating from interstices in the local close packed areas. Silica ceramic with a relative density as high as 73.6 % was thus successfully obtained. This unambiguously proves the potential of the process and the possibility to master the subtle equilibrium between dissolution, precipitation and water release kinetics. However, the experimental approach has to be optimized to make compatible the hydration route and the hydration rate of the green material and its natural close packing. Moreover, the reactivity of the primary particles should be considered as an efficient lever to improve densification.

Acknowledgment

Arnaud Ndayishimiye was supported by a grant from Ministère de l'Enseignement Supérieur, de la Recherche et de l'Innovation.

John F. Wight (Corning Incorporated, New York) is sincerely acknowledged for all fruitful discussions.

References

[1] R.M. German, "Chapter Ten - Sintering With External Pressure" pp. 305–354 in *Sinter. from Empir. Obs. to Sci. Princ.* Edited by R.M. German. Butterworth-Heinemann, Boston, 2014.

[2] L.C. De Jonghe and M.N. Rahaman, "Sintering of Ceramics" pp. 187–264 in *Handb. Adv. Ceram. Mater. Appl. Process. Prop.* 2003.

[3] J.T.M. De Hosson and R. Popma, "Sintering characteristics of nano-ceramic coatings" University of Groningen, 2003.

[4] S. Funahashi, J. Guo, H. Guo, K. Wang, A.L. Baker, K. Shiratsuyu and C.A. Randall, "Demonstration of the Cold Sintering Process Study for the Densification and Grain Growth of ZnO Ceramics" *J. Am. Ceram. Soc.*, **6** 1–6 (2016).

[5] A. Polotai, K. Breece, E. Dickey, C. Randall and A. Ragulya, "A Novel Approach to Sintering Nanocrystalline Barium Titanate Ceramics" *J. Am. Ceram. Soc.*, **88** [11] 3008–3012 (2005).

[6] I.-W. Chen and X.-H. Wang, "Sintering dense nanocrystalline ceramics without final-stage grain growth " *Nature*, **404** [6774] 168–171 (2000).

[7] M. Cologna, B. Rashkova and R. Raj, "Flash Sintering of Nanograin Zirconia in <5 s at 850°C" *J. Am. Ceram. Soc.*, **93** [11] 3556–3559 (2010).

[8] N. Kitamura, Y. Toguchi, S. Funo, I. Kondoh and H. Yamashita, "Density and Refractive Index of Densified Silica Glass" pp. 117–122 in *Hot Isostatic Press. Theory Appl.* Edited by M. Koizumi. Springer Netherlands, Dordrecht, 1992.

[9] R. Chaim, A. Shlayer and C. Estournes, “Densification of nanocrystalline Y_2O_3 ceramic powder by spark plasma sintering,” *J. Eur. Ceram. Soc.*, **29** [1] 91–98 (2009).

[10] J. Majling, P. Znasik, D. Agrawal, J. Cheng and R. Roy, “Conventional and microwave sintering of condensed silica fume” *J. Mater. Res.,* **10** [10] 2411–2414 (1995).

[11] J.D. McClelland, “A Plastic Flow Model of Hot Pressing” *J. Am. Ceram. Soc.*, **44** [10] 526 (1961).

[12] A. Goldstein, R. Ruginets and Y. Geffen, “Microwave sintering of amorphous silica powders” *J. Mater. Sci. Lett.*, **16** [4] 310–312 (1997).

[13] C. Vakifahmetoglu, J.F. Anger, V. Atakan, S. Quinn, S. Gupta, Q. Li, L. Tang and R.E. Riman, "Reactive Hydrothermal Liquid-Phase Densification (rHLPD) of Ceramics. A Study of the $BaTiO_3[TiO_2]$ Composite System" *J. Am. Ceram. Soc.* 99 [12] 3893–3901 (2016)

[14] H. Guo, A. Baker, J. Guo and C.A. Randall, “Protocol for Ultralow-Temperature Ceramic Sintering: An Integration of Nanotechnology and the Cold Sintering Process” *ACS Nano*, **10** [11] 10606–10614 (2016).

[15] J. Guo, H. Guo, A.L. Baker, M.T. Lanagan, E.R. Kupp, G.L. Messing and C.A. Randall, “Cold Sintering: A Paradigm Shift for Processing and Integration of Ceramics” *Angew. Chemie - Int. Ed.*, **55** [38] 11457–11461 (2016).

[16] H. Guo, J. Guo, A. Baker and C.A. Randall, “Hydrothermal-Assisted Cold Sintering Process: A New Guidance for Low-Temperature Ceramic Sintering” *ACS Appl. Mater. Interfaces*, **8** [32] 20909–20915 (2016).

[17] H. Guo, A. Baker, J. Guo, C.A. Randall and D. Johnson, “Cold Sintering Process: A Novel Technique for Low-Temperature Ceramic Processing of Ferroelectrics” *J. Am. Ceram. Soc.*, **99** [11] 3489–3507 (2016).

[18] A. Baker, H. Guo, J. Guo and C. Randall, “Utilizing the Cold Sintering Process for Flexible-Printable Electroceramic Device Fabrication” *J. Am. Ceram. Soc.,* **3** [38709] 1–3 (2016).

[19] F. Bouville and A.R. Studart, “Geologically-inspired strong bulk ceramics made with water at room temperature” *Nat. Commun.*, **8** 14655 (2017).

[20] D.M. Roy, G.R. Gouda and A. Bobrowsky, “Very high strength cement pastes prepared by hot pressing and other high pressure techniques” *Cem. Concr. Res.*, **2** 349–366 (1972).

[21] D.M. Roy and G.. Gouda, “High strength generation in cement pastes” *Cem. Concr. Res.*, **3** [6] 807–820 (1973).

[22] S.-I. Hirano and S. Sōmiya, “Hydrothermal Reaction Sintering of Pure Cr_2O_3” *J. Am. Ceram. Soc.*, **59** [11–12] 534 (1976).

[23] S. Sōmiya, *Hydrothermal reactions for materials science and engineering—an overview of research in Japan.* Springer Netherlands, 1991.

[24] N. Yamasaki, K. Yanagisawa, M. Nishioka and S. Kanahara, “A hydrothermal hot-pressing method: apparatus and application” *J. Mater. Sci. Lett.*, **5** 355–356 (1986).

[25] K. Yanagisawa, M. Sasaki, M. Nishioka, K. Ioku and N. Yamasaki, “Preparation of sintered compacts of anatase by hydrothermal hot-pressing” *J. Mater. Sci. Lett.*, **13** [10] 765–766 (1994).

[26] K. Yanagisawa, K. Ioku and N. Yamasaki, “Formation of Anatase Porous Ceramics by Hydrothermal Hot-Pressing of Amorphous Titania Spheres” *J. Am. Ceram. Soc.*, **80** [5] 1303–1306 (1997).

[27] N. Yamasaki, T. Weiping and K. Jiajun, “Low-temperature sintering of calcium carbonate by a hydrothermal hot-pressing technique” *J. Mater. Sci. Lett.*, **11** 934–936 (1992).

[28] N. Yamasaki, T. Weiping and K. Yanagisawa, “Solidification of $CaCO_3$ containing $SrCO_3$ by hydrothermal hot-pressing” *J. Mater. Res.*, **8** [8] 1972–1976 (1993).

[29] J. Li and T. Hashida, “Preparation of hydroxyapatite ceramics by hydrothermal hot-pressing method at 300 °C” *J. Mater. Sci.*, **42** [13] 5013–5019 (2007).

[30] N. Yamasaki, T. Kai, M. Nishioka, K. Yanagisawa and K. Ioku, “Porous hydroxyapatite ceramics prepared by hydrothermal hot pressing” *J. Mater. Sci. Lett.*, **9** 1150 (1990).

[31] A. Nakahira, S. Takezoe and Y. Yamasaki, “Synthesis of dense Y-zeolite bulks with large surface area using a hydrothermal hot-pressing (HHP) process” *Chem. Lett.*, **33** [10] 1400–1401 (2004).

[32] Y. Xie, S. Yin, H. Yamane, T. Hashimoto and T. Sato, “Low temperature sintering and

color of a new compound $Sn_{1.24}Ti_{1.94}O_{3.66}(OH)_{1.50}F_{1.42}$" *Solid State Sci.*, **11** [9] 1703–1708 (2009).

[33] K. Yanagisawa, M. Nishioka, K. Ioku and N. Yamasaki, "Neck formation of spherical silica particles by hydrothermal hot pressing" *J. Mater. Sci. Lett.*, **9** [1] 7–8 (1990).

[34] K. Yanagisawa, M. Nishioka, K. Ioku and N. Yamasaki, "Densification of silica gels by hydrothermal hot-pressing" *J. Mater. Sci. Lett.*, **12** [14] 1073–1075 (1993).

[35] S. Katsuyama, Y. Takiguchi and M. Ito, "Synthesis of $Ca_3Co_4O_9$ Ceramics by Citric Acid Complex and Hydrothermal Hot-Pressing Processes and Investigation of Its Thermoelectric Properties" *Mater. Trans.*, **48** [8] 2073–2078 (2007).

[36] S. Katsuyama, Y. Takiguchi and M. Ito, "Synthesis of $Ca_3Co_4O_9$ ceramics by polymerized complex and hydrothermal hot-pressing processes and the investigation of its thermoelectric properties" *J. Mater. Sci.*, **43** [10] 3553–3559 (2008).

[37] S. Katsuyama, A. Kishida and M. Ito, "Synthesis of $Na_xCo_2O_4$ by the hydrothermal hot-pressing and its thermoelectric properties" *J. Alloys Compd.*, **414** [1–2] 215–220 (2006).

[38] T. Onoki, K. Hosoi and T. Hashida, "New technique for bonding hydroxyapatite ceramics and titanium by hydrothermal hot-pressing method" *Script. Mater.*, **52** 767–770 (2005).

[39] T. Onoki, S. Yamamoto, H. Onodera and A. Nakahira, "New technique for bonding hydroxyapatite ceramics and magnesium alloy by hydrothermal hot-pressing method" *Mater. Sci. Eng. C*, **31** [2] 499–502 (2011).

[40] K.D. Hartlen, A.P.T. Athanasopoulos and V. Kitaev, "Facile Preparation of Highly Monodisperse Small Silica Spheres (15 to > 200 nm) Suitable for Colloidal Templating and Formation of Ordered Arrays" *Langmuir*, **24** 1714–1720 (2008).

[41] G. Goglio, A. Largeteau, A. Ndayishimiye and M. Prakasam, Procédé et dispositif de densification des matériaux ou de consolidation d'un assemblage de matériaux par frittage hydrothermal ou solvothermal; french patent, submission number 1000405429

[42] J.M.M. Pérez, J. Pascau, *Image Processing with ImageJ*, Packt Publishing (2013).

[43] W.C. Oliver and G.M. Pharr, "Measurement of hardness and elastic modulus by instrumented indentation: Advances in understanding and refinements to methodology" *J.*

Mater. Res., **19** [1] 3–20 (2004).

[44] J.B. Lowe and R.T. Baker, "Deformation of Ordered Mesoporous Silica Structures on Exposure to High Temperatures" *J. Nanomater.*, **2014** ID 754076 (2014).

[45] M. Kruk and C.M. Hui, "Thermally Induced Transition between Open and Closed Spherical Pores in Ordered Mesoporous Silicas" *J. Am. Chem. Soc.*, **130** [5] 1528–1529 (2008).

[46] T.G. Mayerhöfer, Z. Shen, E. Leonova, M. Edén, A. Kriltz, and J. Popp, "Consolidated silica glass from nanoparticles" *J. Solid State Chem.*, **181** [9] 2442–2447 (2008)

[47] J.R. Martinez, F. Ruiz, Y. V. Vorobiev, F. Perez-Robles and J. Gonzalez-Hernandez, "Infrared spectroscopy analysis of the local atomic structure in silica prepared by sol-gel" *J. Chem. Phys.*, **109** [17] 7511–7514 (1998).

[48] S.L. Dean, J.J. Stapleton and C.D. Keating, "Organically Modified Silicas on Metal Nanowires" *Langmuir*, **26** [18] 14861–14870 (2010).

[49] N. Pijarn, A. Jaroenworaluck, W. Sunsaneeyametha, and R. Stevens, "Synthesis and characterization of nanosized-silica gels formed under controlled conditions" *Powder Technol.*, **203** [3] 462–468 (2010).

[50] R.H. Stolen and G.E. Walrafen, "Water and its relation to broken bond defects in fused silica" *J. Chem. Phys.*, **64** [6] 2623 (1976).

[51] J.B.. Bates, R.W.. Hendricks and L.B.. Shatter, "Neutron irradiation effects and structure of noncrystalline SiO_2" *J. Chem. Phys.*, **61** [10] 4163–4176 (1974).

[52] X. Chen, J. Jiang, F. Yan, S. Tian and K. Li, "A novel low temperature vapor phase hydrolysis method for the production of nano-structured silica materials using silicon tetrachloride" *RSC Adv.*, **4** [17] 8703–8710 (2014).

[53] L.T. Zhuravlev, "Surface characterization of amorphous silica—a review of work from the former USSR" *Colloids Surfaces A Physicochem. Eng. Asp.*, **74** [1] 71–90 (1993).

[54] L.T. Zhuravlev, "The surface chemistry of amorphous silica. Zhuravlev model" *Colloids Surfaces A Physicochem. Eng. Asp.*, **173** [1–3] 1–38 (2000).

[55] L. Peng, W. Qisui, L. Xi and Z. Chaocan, "Investigation of the states of water and {OH} groups on the surface of silica" *Colloids Surfaces A Physicochem. Eng. Asp.*, **334** [1–3]

112–115 (2009).

[56] A.K. Soper, "Density Profile of Water Confined in Cylindrical Pores in MCM-41 Silica" *J. Phys. Condens. Matter Phys. Condens.*, **24** 64107 (2012).

[57] K.H. Liu, Y. Zhang, J.J. Lee, C.C. Chen, Y.Q. Yeh, S.H. Chen and C.Y. Mou, "Density and anomalous thermal expansion of deeply cooled water confined in mesoporous silica investigated by synchrotron X-ray diffraction" *J. Chem. Phys.*, **139** [6] (2013).

[58] J. Puibasset and R.J.M. Pellenq, "Water confined in mesoporous silica glasses: Influence of temperature on adsorption/desorption hysteresis loop and fluid structure" *Eur. Phys. J. - Spec. Top.*, **141** [1] 41–44 (2007).

[59] E.A. Wovchko, J.C. Camp, J.A. Glass and J.T. Yates, "Active Sites on SiO_2: Role in CH_3OH Decomposition" *Langmuir*, **11** [7] 2592–2599 (1995).

[60] R.L. White and A. Nair, "Diffuse Reflectance Infrared Spectroscopic Characterization of Silica Dehydroxylation" *Appl. Spectrosc.*, **44** [1] 69–75 (1990).

[61] K.K. Unger, *Porous Silica*. Elsevier Science, 1979.

[62] H. Eckert, J.P. Yesinowski and E.M. Stolper, "Quantitative NMR studies of water in silicate glasses" *Solid State Ionics*, **32** 298–313 (1989).

[63] X. Xue and M. Kanzaki, "Proton Distributions and Hydrogen Bonding in Crystalline and Glassy Hydrous Silicates and Related Inorganic Materials: Insights from High-Resolution Solid-State Nuclear Magnetic Resonance Spectroscopy" *J. Am. Ceram. Soc.*, **92** [12] 2803–2830 (2009).

[64] K. V Romanenko, O.B. Lapina, L.G. Simonova and J. Fraissard, "^{1}H and ^{29}Si-MAS NMR characterization of silicate fiberglass supports" *Phys. Chem. Chem. Phys.*, **5** [12] 2686–2691 (2003).

[65] P. Tekely, "Exploiting ^{1}H ->^{29}Si Cross-Polarization Features for Structural Characterization of Inorganic Materials" pp. 197–203 in *Mod. Magn. Reson.* Edited by G.A. Webb. Springer Netherlands, Dordrecht, 2006.

[66] G. Engelhardt and D. Michel, *High-Resolution Solid-State NMR of Silicates and Zeolites*. John Wiley & Sons Australia, Limited, 1987.

[67] J.P. Rainho, J. Rocha, L.D. Carlos and R.M. Almeida, "^{29}Si nuclear-magnetic-resonance

and vibrational spectroscopy studies of SiO_2–TiO_2 powders prepared by the sol-gel process" *J. Mater. Res.*, **16** [8] 2369–2376 (2001).

[68] A. Ayral, J. Phalippou and T. Woignier, "Skeletal density of silica aerogels determined by helium pycnometry" *J. Mater. Sci.*, **27** [5] 1166–1170 (1992).

[69] D. Sangeeta and J.R. LaGraff, *Inorganic Materials Chemistry Desk Reference, Second Edition*. CRC Press, Boca Raton, New York, 2004.

[70] R. Chaim, M. Levin, A. Shlayer and C. Estournes, "Sintering and densification of nanocrystalline ceramic oxide powders: a review" *Adv. Appl. Ceram.*, **107** [3] 159–169 (2008).

[71] R.M German, *Sintering theory and practice*. Wiley, New York, 1996

[72] S.-T. Hong, Y. Hovanski, C.A. Lavender and K.S. Weil, "Investigation of Die Stress Profiles During Powder Compaction Using Instrumented Die" *J. Mater. Eng. Perform.*, **17** [3] 382–386 (2008).

[73] I. Aydin, B.J. Briscoe and N. Ozkan, "Modeling of powder compaction: a review" *MRS Bull.*, **22** [12] 45–51 (1997).

[74] J.-P. Gratier, D.K. Dysthe and F. Renard, "The role of pressure solution creep in the ductility of the Earth's upper crust" *Adv. Geophys.*, **54** 47–179 (2013).

[75] E.H. Rutter, "The influence of interstitial water on the rheological behaviour of calcite rocks" *Tectonophysics*, **14** [1] 13–33 (1972).

[76] X. Zhang, C.J. Spiers and C.J. Peach, "Compaction creep of wet granular calcite by pressure solution at 28°C to 150°C" *J. Geophys. Res. Solid Earth*, **11** [1] 108–122 (2010).

[77] J.-P. Gratier, R. Guiguet, F. Renard, L. Jenatton and D. Bernard, "A pressure solution creep law for quartz from indentation experiments" *J. Geophys. Res. Solid Earth*, **114** [B3] 1–16 (2009).

[78] J.-P. Gratier, F. Renard and P. Labaume, "How pressure solution creep and fracturing processes interact in the upper crust to make it behave in both a brittle and viscous manner" *J. Struct. Geol.*, **21** [8] 1189–1197 (1999).

[79] I. Shimizu, "Kinetics of pressure solution creep in quartz: theoretical considerations" *Tectonophysics*, **245** [3–4] 121–134 (1995).

[80] G. Vigil, Z. Xu, S. Steinberg and J. Israelachvili, “Interactions of Silica Surfaces” *J. Colloid Interface Sci.*, **165** [2] 367–385 (1994).

[81] K. Kendall, *Molecular Adhesion and Its Applications: The Sticky Universe*. Springer US, 2007.

[82] A. Opitz, S.I. Ahmed, J.A. Schaefer and M. Scherge, “Nanofriction of silicon oxide surfaces covered with thin water films” **254** [2003] 924–929 (2007).

[83] D.H. Everett, “Manual of symbols and terminology for physicochemical quantities and units, appendix II: Definitions, terminology and symbols in colloid and surface chemistry” *Pure Appl. Chem.*, **31** [4] 577–638 (1972).

[84] K. Hirao and M. Tomozawa, “Microhardness of SiO_2 Glass in Various Environments” *J. Am. Ceram. Soc.*, **70** [7] 497–502 (1987).

[85] A. Dutta, D. Penumadu and B. Files, “Nanoindentation testing for evaluating modulus and hardness of single-walled carbon nanotube–reinforced epoxy composites” *J. Mater. Res.*, **19** 158–164 (2004).

[86] F. Fröhlich, P. Grau and W. Grellmann, “Performance and analysis of recording microhardness tests” *Phys. status solidi*, **42** [1] 79–89 (1977).

[87] D. Jauffrès, C. Yacou, M. Verdier, R. Dendievel and A. Ayral, “Mechanical properties of hierarchical porous silica thin films: Experimental characterization by nanoindentation and Finite Element modeling” *Microporous Mesoporous Mater.*, **140** [1] 120–129 (2011).

[88] A. Arora, D.B. Marshall, B.R. Lawn and M. V Swain, “Indentation deformation/fracture of normal and anomalous glasses” *J. Non. Cryst. Solids*, **31** [3] 415–428 (1979).

[89] M. Yamane and J.D. Mackenzie, “Vicker’s Hardness of glass” *J. Non. Cryst. Solids*, **15** [2] 153–164 (1974).